Solar Light-Driven Photocatalysis Using BaFe2O4/rGO for Chlorhexidine Digluconate Contaminated Water: Comparison With Artificial UV and Visible Light-Mediated Photocatalysis

Astha Singh
Indian Institute of Technology (Indian School of Mines): Indian Institute of Technology
Brijesh Kumar Mishra (bkmishra3@rediffmail.com)
Indian Institute of Technolgy (ISM) https://orcid.org/0000-0002-4451-1924

Research Article

Keywords: Chlorhexidine Digluconate, BaFe2O4/rGO, Adsorption combining Photocatalysis, Energy Efficiency

Posted Date: April 28th, 2021

DOI: https://doi.org/10.21203/rs.3.rs-386420/v1

Solar light-driven photocatalysis using $BaFe_2O_4$/rGO for Chlorhexidine digluconate contaminated water: comparison with artificial UV and visible light-mediated photocatalysis.

Astha Singh[a], and Brijesh Kumar Mishra[a]*

[a] Department of Environmental Science and Engineering., Indian Institute of Technology (Indian School of Mines), Dhanbad-826004, India

[a]* Corresponding Author: brijesh@iitism.ac.in

[a] singh.astha0689@gmail.com

Abstract

Synthesis and characterization of dual functioning material is an effective approach for promotion of organic pollutant degradation through adsorption as well as photocatalysis. Herein, graphene oxide modified by addition of barium nitrate and iron to construct smooth sheet-like structure ($BaFe_2O_4$/rGO) for removal of Chlorhexidine Digluconate (CHD). Compare with GO (75.69% -UV-light ;88.17%-visible-light), $BaFe_2O_4$/rGO showed significant adsorption-photocatalysis effect under visible-light (93.95%) than UV-light (78.17%). The introduction of barium nitrate and iron into graphene oxide led to smooth porous structure with increased surface area (93.66 m^2 g^{-1}), which resulted in large number of adsorption active site and great photocatalytic activity with efficient charge separation. Although, catalysts did not mineralize CHD completely, but the parent compound mineralized to some extent, which was confirmed by the TOC measurement and UV_{254} absorbance variation. In addition, toxicity of degraded products was analyzed by bacterial susceptibility test on Bacillus *cereus* DPAML065 suggested that nontoxic byproducts of CHD formed, which led to their safe disposal. Based on the identified transformed products, the possible degradation pathway was proposed. Batch studies demonstrated that $BaFe_2O_4$/rGO is highly photoactive based on reaction rate constant (R^2=0.984), where the kinetics data was well-fitted using the pseudo-first order. Moreover, efficiency of catalysts was examined under solar light to achieve the sustainability.

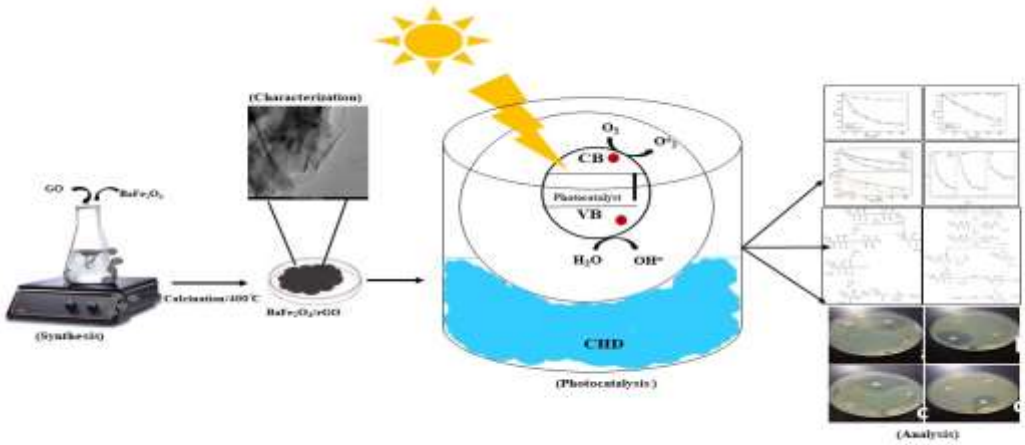

Keywords: Chlorhexidine Digluconate; $BaFe_2O_4$/rGO; Adsorption combining Photocatalysis; Energy Efficiency

Highlights

- The adsorption and photocatalysis efficiency of $BaFe_2O_4$/rGO as catalyst displayed excellent degradation performance to CHD through π-π stacking.
- Reduction in UV_{254} also confirmed that the mineralized end product by $BaFe_2O_4$/rGO has excellent degradation efficiency.
- Photogenerated electrons and Hydroxyl radicals was substantially responsible for CHD degradation.
- Toxicity of parent compound and its by-products reduces after photocatalysis process in $BaFe_2O_4$/rGO and possible pathway were established.

1. Introduction

Extensive research has focused on photocatalytic degradation of Personal Care Products (PCPs) due to their recalcitrant nature, nonbiodegradability, and unregulated disposal into aquatic bodies.These compounds, thus, negatively impact on both environment and human health (Das et al., 2014). Chlorhexidine Digluconate (CHD), which is a model compound, is broadly used as antiseptic among PCPs. It is commonly present in disinfectant, mouthwash formulations, toothpaste and cosmetics due to effectiveness against Gram-positive and Gram-negative bacteria (Sousa et al., 2017). CHD consist

of two hexanes bonded (p-chlorophenyl) biguanides and its primary degradation product p-chloroaniline act as a limiting factor for stabilizing the compound. However, overuse of these compound have been frequently detected in water bodies and are quickly absorbed/ metabolized as both hemotoxic and carcinogenic(Nidhi et al., 2011). Due to complex structure and bacteriostatic properties of CHD molecules, it can neither be completely removed through conventional treatment technologies from wastewater nor be biodegraded from the environment (Zwiener and Frimmel, 2000).

Thus, the development of efficient technologies are highly desired to remove PCPs and pharmaceuticals such as CHD from the aquatic ecosystem (Fidelis et al., 2019). Adsorption is an efficient and economical treatment for organic pollutant but with some limitations such as inefficient in complete degradation and leads to the secondary pollutant. Recently, graphene oxide (GO) with high surface area, strong functional group and conjugate π region used as an adsorbent for organic pollutant removal (Zhang et al., 2016).Undoubtedly, adsorption process can only change the phase of the pollutant, cannot completely remove the organic pollutant. In addition, photocatalysis is an efficient and green technology for mineralization of recalcitrant organic pollutant with some advantages such as lack of secondary waste generation and easy implementation (Wang et al., 2021). Interestingly, studies showed that use of adsorption-photocatalysis simultaneously grab attention for efficient removal of organic pollutant due to recombination of electron-hole pair disadvantage of photocatalysis (Yuan et al., 2020). Various studies showed significant removal of antibiotics using adsorption-photocatalysis treatment such as ciprofloxacin (with 59.5% adsorption and 82.5 % degradation in 60 min), tetracycline (with 18% adsorption and 70% degradation in 90 min), ofloxacin (with 93.4% adsorption and photocatalytic degradation in 30 min) (Chen et al., 2020).Motivated by previous studies, Barium ferrites with exceptional magnetic and photocatalytic property used for synthesis of new material in order to develop the dual functioning material by combining the advantages of both adsorption-photocatalysis technologies (Roonasi and Mazinani, 2017a). As per the literature, barium ferrites have less been studied and can also be used for easy separation as well as strong visible light absorption capacity due to narrower band gap (Casbeer et al., 2012).

In this system, Response surface methodology (RSM) has been used to understand the interaction among the operating conditions (pH, catalyst dose and time) for optimization process, resulting in a good estimate of the optimum response $BaFe_2O_4$/rGO used as an adsorbent first in dark, and as photocatalyst under UV, visible and solar radiation. In addition, kinetic studies for removal of pollutant, mineralization rate (in terms of TOC) and reduction in aromaticity (in terms of UV_{254}/UV_{280}) during adsorption and photocatalysis has been carried out. Furthermore, possible mechanism for mineralization of pollutant via adsorption-photocatalysis was studied by trapping experiment and possible pathway was proposed, based on LC-MS analysis. For practical applicability,

$BaFe_2O_4$/rGO photocatalyst used for the treatment of formulated wastewater in UV, visible and solar radiation.

2. Materials and Methods

2.1. Chemicals

All the chemicals and reagent were procured by Sigma-Aldrich. They were of analytical grade and used without further purification. Microporous hydrophobic PTFE membrane with pore size around 0.45 μm and 80 % porosity was obtained from GE Osmonics Company.

2.2. Syntheses of Graphene Oxide:

For the present study, 1 g of graphite (Jodex England) was carefully added to the mixture of concentrated H_2SO_4:H_3PO_4 (prepared in a ratio of 4:1 by v/v). After the addition of graphite, the prepared solution was placed in an ice bath. Consequently, the experimentation was carried out at room temperature where the prepared mixture was stirred for 72 h using a rotary shaker. The process was carried out till the mixture's color changed to dark brown from dark purplish green. H_2O_2 was added to the mixture to halt the oxidation process, which further changed its colour to bright yellow. Moreover, remnant salts in the mixture were removed by adding of 10% HCl. The washing process for the experimentation followed a simple decantation of supernatant. It was observed that during the process of washing, the addition of deionized water caused exfoliation of GO, which thickens the solution due to the formation of GO gel. The obtained GO gel was further dried for 24 h at 70 ºC. The dried GO gel was then stored in a dry place for further experimentation (Aboubaraka et al., 2017).

2.3. Synthesis of $BaFe_2O_4$/rGO

A certain amount of Barium nitrate and iron (2:1 w/w) were added into 100mL beakers using distilled water at 60℃. To this mixture, prepared graphene oxide was added in mass ratio of 1:2 w/w. Afterward, the resulting suspension kept at magnetic stirrer for homogeneous mixing. Then, the solution was filtered and ignited at a temperature of 400 °C for 30 min. The resultant dark brown material was obtained and powdered into fine particle (Roonasi and Mazinani, 2017b).

2.4 Characterization

To prove the stability of prepared sample as a photocatalyst, following characterization were employed i) X-ray diffraction (XRD) was used for phase identification on a Bruker D8 ADVANCE diffractometer with Cu-Kα (λ=1.5406 Å) radiation, ii) Fourier transform infrared (FTIR) spectra was used to identify the presence of functional group on Bruker Vertex- 70 by diffused reflectance accessory technique, iii) morphology and structural observations were analyzed using Hitachi S-4300

type field emission scanning electron microscope (FE-SEM) at an electron acceleration voltage of 1 keV, iv) Energy-dispersive X-ray spectrometer (EDX) equipped on SEM was used to identify the chemical compositions and elemental mapping of the catalyst, v) UV–vis diffuse reflectance spectra (UV-DRS) was used for bandgap analysis using Perkin Elmer Lambda 900 spectrophotometer equipped with an integrated sphere ($BaSO_4$ was used as a reference material),and vi) X-ray photoelectron spectroscopy (XPS) was used to identify the oxidation state of compounds using a VG 250 Escalab spectrometer equipped with an Al anode (Al-Kα=1486.7 eV) as an X-ray source.

2.4. Experimental Design using Response surface Methodology

RSM was used to optimize three variables (s/c ratio, pH and time) with three different levels (+1, 0 and -1) for maximum CHD removal as a response. The experimental design (DoE) was performed based on the Face Centred Central Composite Design (FCCD) devised by Design Expert v7.0.0 software (SaMeep 104, State Ease, INC. Minneapolia (USA). A total of 20 different combinations were obtained with six centre points in random order according to a Central Composite Design (CCD) configuration for three factors. In this analysis, Face Central Composite Design (FCCD) was used to model the percentage removal of CHD as a quadratic model. "Analysis of variance" (ANOVA), correlation coefficient (R^2), lack of fit, CV % and adjusted coefficient of determination (R^2_{adj}) were used for statistical validation.

2.5.Adsorption experiments

The adsorption kinetics has been performed for the adsorbent in dark condition at optimized condition. At a certain time- interval, suspension was collected and filtered through 0.45µm syringe filter. The residual concentration of CHD was measured in UV-vis spectrophotometer (Lab-tech, China). The adsorption capacity at equilibrium (q) was determined as

$$q = (C_o - C_e)V/m \quad (1)$$

where C_0 and C_e (mg L^{-1}) are the initial and equilibrium pollutant concentrations, respectively, V represented the solution volume (L), and m (g) is the adsorbent mass.

The pseudo first-order kinetic model was given by:

$$\ln (q - q_t) = \ln q - k_1 t \quad (2)$$

where t is time, q_t is adsorption capacity at time t, and k_1 is the pseudo-first-order rate constant.

The pseudo-second-order kinetic model was given by:

$$\frac{t}{q_t} = \frac{t}{q} - \frac{1}{k_2 q^2} \quad (3)$$

where k_2 is the pseudo-second-order rate constant.

2.6.Photocatalytic activity test

The photocatalysis activity during CHD degradation was monitored in a lab-scale photoreactor under UV light (PMI, India). The source of light provided by a UVC-lamp (11W, Phillip, intensity-44.4 $mW.cm^{-2}$) and visible lamp (200W, intensity- 40 $mW.cm^{-2}$) and natural light (intensity -50-60 $mW.cm^{-2}$) was measured by a radiometer (Delta OHM, LP-NET14). The dispersion of catalyst in a 500 mL solution of CHD (30 ppm) was injected into the photoreactor with aeration and operational condition (pH range 6-10, S/C ratio 1.01-3.0 and Time 10-60 min.). This experiment tracked and analysed the residual CHD in the reaction mixture as a function of time. To check the experimental results' reproducibility, all the experimental runs were repeated three times. Where, one-hour batch study was conducted with sample collection at a 5-minute interval. An aliquot was centrifuged (4℃, 11,000 X *g*, 5 min.) and the supernatant was collected for subsequent analyses.

2.7. Kinetic study of CHD degradation

Calculating oxidant and reductant in solution is nearly impossible. Thus, the kinetic pseudo-first-order model has been carried out to study the modeling CHD degradation Eqs (4) & (5).

$$\ln \frac{C_t}{C_O} = -K_{obs} t \quad (4)$$

$$r_{obs} = -k_{obs} C_{CHD} \quad (5)$$

Where, K_{obs} (Rate constant of reaction) was calculated from the slope by plotting a graph between $\ln \frac{C_t}{C_o}$ versus t and r_{obs} is the observed CHD degradation rate (mg L^{-1} min) in the photoreactor. In the above equations, the reaction rate constant (K_{obs}) can be either negative or positive. Noticeably, " K_{obs} " does not include the concentration as these parameters are taken into consideration (Nasseh et al., 2018).

2.8. Analytical Method

UV–vis spectrophotometer (Lab-tech, China) was used to measure the Ultraviolet (UV) absorbance at 254 nm, 280nm and residual CHD concentration in the reaction mixture were measured at 275 nm upon the specification of spectral indices. TOC analyzer (Shimandzu 5000) was used to determine the reduction of organic content and mineralization of CHD. LC-MS analysis (Thermo Scientific TSQ 8000 liquid chromatograph-mass spectrometer) has been carried out to investigate the degradation products of CHD.

The figure-of-merit electrical energy per order (EEO) is useful for evaluating electrical energy consumption in photocatalytic degradation of organic contaminants, as per International Union of Pure and Applied Chemistry (IUPAC). EEO defined as amount of electrical energy consumed (kWh) during photocatalytic degradation of fixed volume of organic pollutant (Azarpira et al., 2019).

$$E_{EO} = \frac{P \times t \times 1000}{V \times 60 \times \log \frac{C_i}{C_f}} \quad (6)$$

Where P is the power rate (kW) of the photocatalytic system, t is the irradiation time (min), V is the volume (L) of the sample.

2.9. Bacterial susceptibility test for CHD degradation and photo mineralized product

A bacterial susceptibility test was carried out on anaerobic gram-positive bacteria (*Bacillus cereus)* to evaluate the potential for aquatic toxicity of treated and untreated CHD containing water. The susceptibility test was carried out by autoclaving agar media of Muller Hinton, and Petri plates at 66.8Pa and 121℃ for 20 min. Approximately 1ml of cultural broth suspension of *Bacillus cereus* were mixed in a media. Homogeneously mixed cultural suspension of bacteria and media shows a confluent lawn of growth on incubation. The incubation period for bacterial growth was carried out for 24hr at 37℃ prior to observation of the inhibition zone.

3. Results and discussion

3.1 Characterization of the synthesized photocatalyst

The synthesized catalysts were characterized to know the bandgap, surface morphology, elemental analysis, and crystallinity. UV-vis diffuse reflectance spectroscopy was used to determine optical absorbance property of prepared sample and their light-harvesting nature in the wavelength visible range (200-800 nm). Both the GO and $BaFe_2O_4$/rGO can absorb visible light but $BaFe_2O_4$/rGO shows strong absorption in visible range due to the shifting of red absorption peak and low bandgap energy was calculated using the following formula:

$$E_g(eV) = \frac{1240}{\lambda_g} nm$$

Where λ_g is the wavelength value obtained from UV-DRS spectra. The bandgap energy has been calculated from Tauc plot of absorbance data (Fig.1c), which show the improvement of the photocatalytic performance of both synthesized photocatalyst (GO and $BaFe_2O_4$/rGO). The lowering of band energy in GO (2.89eV) and $BaFe_2O_4$/rGO (1.86 eV) showed that the synthesis process has been achieved successfully. DRS results of GO revealed the absorption peak of $\pi \rightarrow \pi^*$ transition of C-

C bonds around 210-203 nm along with another peak of n→π* transition of C-O bonds around 300-320 nm. However, in $BaFe_2O_4$/rGO, π→π* transition peak has been shifted around 260-270 nm demonstrating the restoration of electronic conjugation on functionalization of GO. Therefore, $BaFe_2O_4$/rGO can effectively improve the light absorption properties of GO, for visible range as well.

Fig. 1: a) XRD patterns; b) FTIR spectra and c) UV-vis diffuse reflectance spectra of GO and $BaFe_2O_4$/rGO.

FTIR spectrum was recorded to verify the successful synthesis of photocatalyst. Compared the spectrum of pure GO and $BaFe_2O_4$/rGO , the GO (Fig.1b) shows the characteristic peaks around 1734 cm^{-1} (due to the presence of -COOH), 1580 cm^{-1} (C=C vibration form graphitic domain), 1375 cm^{-1} (-C-OH), 1232 cm^{-1} (C-O stretch) and 1050 cm^{-1} (epoxide groups), respectively. These patterns further confirm the presence of oxygen containing functional group of GO. Furthermore, a broad and less intense peak in the region around 3500-3000 cm^{-1} was also observed due to stretching vibrations of hydroxyl group from absorbed water molecules or phenolic OH or OH from carboxylic groups in GO.As for $BaFe_2O_4$/rGO (Fig.1b), the characteristic peaks of oxygen-containing functional groups of GO disappear and single sharp peak appeared at band 1420.31 cm^{-1} reveals the metal-oxygen characteristic (Roonasi and Mazinani, 2017a) and reduction of GO to rGO occurred. By comparing the two curves (GO and $BaFe_2O_4$/rGO), it was found that the characteristic peaks of GO are weakened in $BaFe_2O_4$/rGO and confirmed the synthesis was done successfully (Sonal et al., 2020).

Diffusion peaks from XRD analysis of GO (Fig.1a), was found at $2\theta = 10.46^{\circ}$ (001) with d-spacing of 0.850 nm due to the oxidation of graphite. The published studies suggested that the characteristic peak of graphite found at $2\theta = 26.58^{\circ}$ (002) would disappeared due to the addition of oxygen-containing functional group (Aboubaraka et al., 2017). Thus, suggesting that GO was successfully synthesized. In addition, the intensity and sharp diffraction peak was observed at $2\theta=32^{\circ}$ with interlayering spacing 0.27nm indicating the presence of metal on the surface of carbon (Roonasi and Mazinani, 2017a). Besides this peak, characteristic peak of GO at $2\theta =10.46^{\circ}$ was disappeared and a weak peak found at $2\theta = 28.43^{\circ}$, corresponding to coexistence of Ba^{2+} on the surface of GO in $BaFe_2O_4$/rGO (Fig.3a) (Roonasi and Mazinani, 2017a). Therefore, the results from XRD analysis confirmed the crystallographic nature of material and the coexistence of Ba^{2+} and GO.

XPS data used to detect the chemical constituents of GO and $BaFe_2O_4$/rGO. The corresponding peaks of C 1s, O 1s, Ba ($3d_{5/2}$), ($3d_{3/2}$) and Ba (4d) were identified in both the sample. More specifically, high-resolution of C 1s spectra of GO showed peaks at 284.6, 285.3, 288.0, and 289.2 eV (Fig.2), which correspond to C-O and C=O bonds respectively (Bai et al., 2018). Additionally, with the formation of $BaFe_2O_4$/rGO, band energies of C (1s) was decreased approximately to 284.68 eV, indicating reduction of oxygen-containing functional group and confirming the transformation of GO to rGO with the doping on sp^2 carbon atom of GO (Hu et al., 2020). Similarly, peak of O 1s found at

532.86 eV is attributed to the lattice of O or -OH group on the surface of GO, respectively (Hu et al., 2020).While, O1s core level spectrum of $BaFe_2O_4$/rGO was deconvoluted at 530.68 eV ($BaCO_3$), suggesting the presence of Ba^{2+} on the surface of GO (Han et al., 2021). This shifting of band energies shows the interaction of GO and $BaFe_2O_4$ and their influence on the hydroxyl oxygen of the surface. Evidently, the double peak of Ba ($3d_{5/2}$), ($3d_{3/2}$) and Ba (4d) appeared at binding energies of 779.60 eV, 794.90 eV and 89.84 eV, respectively on the surface of C1s, indicated the successful formation of $BaFe_2O_4$/rGO (Fig.2) (Han et al., 2021).

Fig 2: a) Full scan spectra and extended high-resolution b) C 1s; c) O 1s and d) Ba 3d spectra of GO and BaFe2O4/rGO

The surface and structural morphological were investigated by SEM and high-resolution TEM (HRTEM). As shown in Fig.3a-e, GO consist of the two-dimensional, grooved and undulated sheet-like structure due to deformation upon exfoliation and restacking of graphite. This inner layering of GO occurs due to the presence of oxygen-containing functional groups such as carboxyl, epoxy and hydroxyl group was also supported by FTIR analysis. While, $BaFe_2O_4$/rGO (Fig.3f-m) have smooth sheet like morphology with more corrugations as compared to the GO. The elemental analysis confirmed the presence of C, O and Ba in the samples with other adhering impurities and also proved the successful introduction of Ba in GO (Aboubaraka et al., 2017; El-Sheikh et al., 2017; Wang et al., 2012). In addition, TEM images and elemental mapping of prepared photocatalyst confirmed the uniform distribution of C, O, Fe and Ba throughout the material.

Fig 3: SEM, TEM and EDS images of photocatalysts (a-e) GO; and (f-m) $BaFe_2O_4$/rGO.

The BET surface area of GO and $BaFe_2O_4$/rGO are 93.66 66 m^2g^{-1} and 91.50 m^2g^{-1} , respectively. A large surface area is widely believed to be needed for high photocatalytic process. In contrast, $BaFe_2O_4$/rGO possess low surface area as compared to GO but shows high photocatalytic activity. The possible reason was the presence of potential reactive sites and shortening of mass transfer distance, enhance the adsorption and photocatalytic process (Zhu et al., 2018).

Therefore, this characterization studies suggested that use of GO and $BaFe_2O_4$/rGO proved as efficient photocatalyst because various oxygen-containing functional group participates in redox reaction and polyaromatic π-system of GO and $BaFe_2O_4$/rGO reacts with the aromatic rings of CHD in wastewater by either π−π stacking interactions or strong hydrophobic effect make them highly efficient adsorbent materials as well (Thakur and Kandasubramanian, 2019).

3.2 Regression analysis for the photocatalytic activity of photocatalyst on CHD removal

A polynomial model was used to represent the effects of individual parameters as well as their synergistic interactive effects on the response variable in Eq. (8)-(9).

290 $$\text{CHD removal \% (GO)}\ \gamma = 55.34 - 2.07\,X_1 + 10.16\,X_2 + 4.25\,X_3 - 2.26\,X_1X_2 + 0.39\,X_1X_3 + 0.74\,X_2X_3 - 13.95\,X_1^2 - 4.34\,X_2^2 - 6.26\,X_3^2 \quad (8)$$

291

292 $$\text{CHD removal \% } (BaFe_2O_4 / rGO) = 44.67 - 1.51\,X_1 + 9.67\,X_2 + 3.52\,X_3 - 1.81\,X_1X_2 - 0.043\,X_1X_3 - 0.3\,X_2X_3 - 11.99\,X_1^2 - 3.29\,X_2^2 - 1.64\,X_3^2 \quad (9)$$

293

294 The results of ANOVA (Table 1) represent the suitable model for photocatalysts during photocatalysis
295 process. The P-value of the model, for the photocatalysts, was <0.0001, and the F-value was 27.27
296 and 63.49 for GO and $BaFe_2O_4$/rGO, respectively. These results confirmed that the model was highly
297 significant, which is supported by the close agreement between the predicted and observed values
298 (Fig.S1: A-B in supplementary material). The R^2 values were obtained 0.9609 and 0.9828 for GO and
299 $BaFe_2O_4$/rGO, respectively, which implies high correlation between actual and predicted values for
300 CHD removal and further confirmed the reliability of model (Sonal et al., 2018). Smaller P > F (<
301 0.05) values show the significance of the certain model and the higher contribution towards the
302 response variable, while the higher P-value indicates the insignificance of the model.

303 **Table 1**: ANOVA Analysis for the catalytic activity of the different photocatalyst

304

305 ***3.3 Adsorption and Photocatalytic performance of prepared photocatalysts***

306 Comparison of adsorption in dark condition, photolysis and photocatalysis were carried out at RSM
307 optimized condition (Fig.4). Adsorption studies were carried out in dark condition and remarkable
308 results was observed with adsorption equilibrium at 80 min and 60 min for GO and $BaFe_2O_4$/rGO,
309 respectively. Kinetics studies of different sample demonstrated a pseudo- second order model is better
310 fitted with experimental and calculated results. Adsorption capacities of $BaFe_2O_4$/rGO and GO are
311 303.3 mg/g (within 60 min) and 200 mg/g (within 80min), respectively. The adsorption capacity of
312 GO enhanced by addition of $BaFe_2O_4$, resulted in increased surface area in $BaFe_2O_4$/rGO as
313 determined by BET. However, above result indicated that $BaFe_2O_4$ loading was beneficial for
314 adsorption of CHD as representative of organic pollutant. This is due to the electrostatic interaction,
315 π-π stacking and more disorder region in $BaFe_2O_4$/rGO than GO (Singh et al., 2018). Point zero
316 charge of GO (6.0) and $BaFe_2O_4$/rGO (4.8) (Fig.S2), this may be due to the presence of carboxyl
317 group and metal-oxygen group in GO and $BaFe_2O_4$/rGO. Highest degradation rates were observed,
318 when solution pH was equal to alkaline condition due to the electrostatic interaction occur among
319 cationic nature of CHD and positively charged photocatalyst. Thus, adsorption occurs due to the
320 electrostatic interaction of pollutant on the surface of photocatalysts, making good agreement for
321 adsorption of antibiotics.

322 **Fig 4:** a) Adsorption of CHD at optimized condition; b) pseudo-first order model; and c) pseudo-
323 second order model for GO and $BaFe_2O_4$/rGO

In addition, agglomeration and surface hydrophobicity are the major limitation for modification of GO and several researches were conducted to modified surface of GO via doping, fabrication, or immobilization for improvisation of these shortcomings. Therefore, grafting of Ba^{2+} on the surface of GO aimed to realize separation, dispersity, high antibiotics adsorption capacity (Li et al., 2019).

The photodegradation efficiency of both materials were compared under visible light irradiation for CHD (Fig.5a). First, blank experiment (photolysis) was performed in visible-light (370-420 nm) and slight degradation of CHD (10%). The adsorption-desorption equilibrium experiment was carried out in dark for stability of the photocatalytic reaction. It was observed that photocatalyst showed negligible degradation in absent of light. Moreover, it was found that the increased adsorption efficiency could also be favourable for photocatalytic activity i.e., GO (88.17%) and $BaFe_2O_4$/rGO (93.95%) for CHD removal. Since, adsorption process decreased the mass transfer distance among pollutant and photocatalyst. Meanwhile, narrow band-gap energy, homogeneous dispersion, and excellent electrical conductivity leading to the significant interaction of d-d (from 3d orbital of Ba ions) and d-π transitions (aromatic rings of CHD molecules) under visible-light formed by photogenerated carrier with short time and pollutant. Additionally, pseudo-first order (PFO) kinetics was in good agreement with reaction rate constant 0.954 (GO) and 1.14 ($BaFe_2O_4$/rGO), respectively. While corelation coefficient of the model (PFO) are 0.937(GO) and 0.984 ($BaFe_2O_4$/rGO), respectively i.e. closer to 1.

Reusability test carried out to investigate the large-scale applicability of photocatalyst as an industrial use. The rate of CHD degradation by $BaFe_2O_4$/rGO decreased after 4 cycles, indicating that $BaFe_2O_4$/rGO possessed good reusability.

Thus, above results suggested the $BaFe_2O_4$/rGO showed optimal balance for adsorption and photocatalytic process as compared to the GO and also considered as durable photocatalyst.

Fig 5: a) Photocatalytic degradation of CHD at optimized condition; b) pseudo-first order kinetics; c) trapping experiment of active species; and d) reusability experiment of GO and BaFe2O4/rGO mediated photocatalytic degradation of CHD.

3.4 Probable mechanism for CHD degradation

Charge separations occur on the surface of photocatalysts (GO and $BaFe_2O_4$/rGO) by exposure of visible-light irradiation. The photogenerated electron and photogenerated holes migrates to the surface of photocatalyst, where they participate in redox reaction for degradation of targeted pollutant. As photodegradation efficiency of photocatalyst is related to the contribution of its active radicals (Fig.5c). A series of trapping experiments were carried out and isopropanol (IPA) (1%), 1.0 mM of potassium persulfate ($K_2S_2O_8$) and ethylenediaminetetraacetic acid (EDTA) were used as scavengers of hydroxyl radicals (^oOH), electron (e^-), and holes (h^+) respectively. The photocatalytic efficiency of

GO and $BaFe_2O_4$/rGO was reduced by addition of IPA and $K_2S_2O_8$ and insignificant change was observed on EDTA addition. However, ^oOH and e^- actively participate in photocatalytic degradation of CHD in GO and $BaFe_2O_4$/rGO mediated photocatalytic reaction but h^+ has insignificant effect, respectively. The removal rate reduced from 88.17 % to 67.44 (IPA),55.81(EDTA) in the case of GO mediated photocatalysis process, while in $BaFe_2O_4$/rGO mediated photodegradation of CHD decreased rapidly from 93.95 % to 75.19% (IPA) and 63.56% (EDTA), respectively. This result indicates that IPA and $K_2S_2O_8$ inhibited the CHD degradation and further confirms that ^oOH and e^- was dominating reactive species. Above result speculated the effect of photogenerated reactive species decreased in order of $e^- > {}^oOH > h^+$.

The photogenerated electron (valance band) and holes (conduction band) participate in redox reaction, where holes may react with water molecules or OH^- to produce ^oOH and photogenerated electron at conduction band may reacts with oxygen to produce superoxide radical anions (O_2^-) (Fig.5c). As CHD (cationic in nature) reacts with ^oOH and e^-, then oxidation process takes place in degradation of pollutant.

Performance and application of the any catalyst depends on degradation and mineralization of the targeted compound into nontoxic smaller molecules. Therefore, it is important to understand the CHD degradation to 88.17 % (GO) and 93.95 % ($BaFe_2O_4$/rGO) by:

a) TOC determination, which shows the relationship between mineralization of pollutant and b) formation of its by-products. The TOC values were reduced to 79.21% and 88.14% for GO and GO-$BaFe_2O_4$/rGO, respectively showing the extent of mineralization taking place in the reaction solution (Fig.6a). Difference in the values of TOC reduction and degradation of CHD, reflects the presence of carbon atom as by-products in treated water (Chen et al., 2020). This result supported with reduction in hydrophobic compound and conversion of heteroatoms such as chlorine or nitrogen into inorganic anions in solution was also determined to investigate the photocatalytic efficiency of catalysts. UV_{254} is the crucial parameter to determine the cleavage of aromatic C=C in solution after photocatalysis process. Thus, reduction in the value of aromatic C=C content present in CHD with respect to time was measured at 254 nm in UV-Spectroscopy (Priya et al., 2018). UV_{254} reduction was ranging from 1.369 to 0.668 and 0.397 for GO and $BaFe_2O_4$/rGO, respectively. This reduction is stoichiometrically close to the removal percentage of hydrophobic compound using (GO) 57.19 % and 71.09% ($BaFe_2O_4$/rGO) (Fig.6b). Hence, UV_{254} reduction confirm the breakdown of long chain carbon atoms into smaller molecules. But 57.19 % in GO mediated treatment indicates that breakdown of CHD into transformed product i.e.p-chloroaniline validated by LC/MS has adverse effect on aquatic life than parent compound .Similarly, inorganic ions production and TOC reduction supports the results of UV_{254} reduction. From this, it could be hypothesized that oxidative mechanism of photocatalysis process participate in cleavage of the aromatic ring of CHD molecules (Schneider et al., 2014).

Therefore, result showed that GO and $BaFe_2O_4$/rGO also has immense potential to reduce aromaticity of the solution.

The overall reaction during photo mineralization of CHD in the excess of oxygen under optimized experimental condition is validated by the equation given below:

$$C_{34}H_{54}Cl_2N_{10}O_7 + 36O_2 + h\nu\ (370\text{-}400\ nm) \rightarrow 34CO_2 + 10NH_3 + 2HCl + 11H_2O \qquad \text{Eq (7)}$$

Besides the TOC and aromaticity reduction, in order to explicate the route of CHD conversion into intermediates of the reaction, the sample was subjected to various experimental condition concerning i) the presence of chloride ion in the reaction mixture, ii) release of attached nitrogen into ammonia ion.

Fig 6: a) TOC removal and b) UV absorbance reduction in GO and $BaFe_2O_4$/rGO mediated photocatalytic degradation of CHD at optimized condition.

The initial concentration-time profiles of chloride anion and inorganic nitrogen (NH_4^+) for photocatalytic system shows significant conversion of organic chlorine to chloride anion in GO and $BaFe_2O_4$/rGO mediated CHD removal. It was observed that there was a formation of approximately, 0.7748 mg/L and 0.7814 mg/L chloride ion respectively, in the reaction matrix of GO and $BaFe_2O_4$/rGO treated water. A similar trend was also observed for the attached nitrogen where, 75.96% and 78.56% N-NH_3 (stoichiometric amount) formation was observed in the case of GO and $BaFe_2O_4$/rGO treated wastewater, respectively.

b) Secondly, bacterial susceptibility test was carried out regarding the toxicity of intermediate. For toxicological studies of intermediate compound targeted microorganism was *Bacillus cereus*, which is commonly residing in human oral cavities was subjected to antimicrobial susceptibility test for toxicity investigation of the intermediate compound. Kirby–Bauer Disk Diffusion method was used to demonstrate toxicological results of the degraded compound. The zone of inhibition (measured in millimetres) of the treated sample through photocatalysts were observed on their respective plates. The diameter of the inhibition zone related to the susceptibility of *Bacillus cereus* and the diffusion rate of pure sample to the antibiotics such as amoxicillin and ciprofloxacin through agar media. Inhibition zone of a standard solution of CHD, 30 mg/L concentration of sample, ciprofloxacin and amoxicillin antibiotics was 30 mm, 15 mm, 50 mm and 3 mm in diameter (Fig.S3). Negligible inhibition zone was observed for the degraded product after photocatalytic degradation of CHD. The pattern of inhibition zone found after preliminary toxicological test on microorganisms without any preclinical analysis of CHD, illustrates the superiority of antimicrobial activity of pure CHD over ciprofloxacin and amoxicillin. From toxicological studies, it was observed that disposal of treated

water into the environment was non-toxic in nature or unlikely to cause any harmful effect on the aquatic ecosystem.

Hence, formation of these mineralized products as well as degradation rate of CHD indicates the extent of true mineralization process. Higher degradation of CHD was achieved using $BaFe_2O_4$/rGO as compared to GO, this could be due to the dispersion of photocatalyst in water and enough availability of active site to irradiate through visible light led to the generation of enough ^{o}OH for noticeable mineralization of CHD. This stoichiometrically estimated values of formed chloride anion is close to the chlorine attached to the ring of CHD in untreated water (1.438 mg/L). Therefore, this estimation degraded products such as chloride ion or nitrogen moieties validates the mineralization of CHD by chloride ion formation.

In this context, degraded product analysis was carried out by LC-MS spectroscopy. Spectral peaks reflect the main intermediate formed during degradation of CHD and thus the toxicological investigation of degraded products has been carried out. The spectral reflection of pure chlorhexidine at 505 and 507 m/z shows two isotopes of Cl atoms (35 and 37) present in the structure.

Whereas in case of GO, fragmentation of the parent molecules into smaller molecules represented by spectral peak (m/z = 127) with some noise shows the reduced number of byproducts, confirming 75-79% of the mineralization process. In $BaFe_2O_4$/rGO mediated photocatalytic degradation, fragmentation of CHD into intermediates represented by one minor peaks (m/z = 149) with reduced number of intermediates (Table 2). A possible pathway for degradation of CHD by catalysts was proposed and breakdown of biguanide moiety found as a major contributor for the mineralization of CHD. Due to the breakdown of biguanide moiety, hydrolytically sensitive group of CHD involves the hydration and subsequent cleavage of C=N bond which leads to the conversion of parent compound to transformed products. In addition, quantification and mass identification of transformed product are beyond the scope of study and would hopefully be addressed in a future study.

Table 2: LCMS Analysis of GO and $BaFe_2O_4$/rGO mediated photocatalytic degradation of CHD.

3.6 Evaluation of photocatalytic efficiency of catalysts in UV and solar treatment.

To evaluate the efficiency of photocatalyst with ultimate goal of solar treatment for removal of organic pollutant. For this purpose, GO and $BaFe_2O_4$/rGO were used for CHD removal under solar as well as UV-light. First, photodegradation were carried out under the UV-irradiation and solar light at RSM optimized condition for the sake comparison with visible-treatment (Wang et al., 2019). These results justify the remarkable potential of photocatalysts for degradation of CHD using solar light to maintain the sustainability. The removal efficiency of GO and $BaFe_2O_4$/rGO for CHD degradation under solar irradiation in terms of UV absorbance and TOC showed in (Table 3). The results highlighted the superior performance under UV light as compared to solar as well as visible. Thus, solar possess combination of UV and visible was beneficial to accelerate the removal of such

recalcitrant pollutant. Energy consumption and economics are of paramount importance for treatment technologies.

Table 3: Comparison of CHD degradation using GO and $BaFe_2O_4$/rGO under different source of light.

3.7.Electrical energy consumption

Electrical energy consumption is also one of the important factors for selection of water treatment technology and its industrial applicability. Since photocatalytic degradation is an electric-intensive process for the removal of recalcitrant organic pollutant. Although, consumption of electrical energy is major representative of operating cost, quality goal and economics on large-scale. In this work, efficiency of treatment process based on electrical energy consumption was quantified using the concept of figure-of-merit electrical energy per order (Eq.-6). For visible treatment, the calculated EEO for GO mediated photodegradation was in the range of 20.09-29.95 (kW h L^{-1} $order^{-1}$), which shows more consumption than $BaFe_2O_4$/rGO mediated visible treatment (16.08 to 22.79 $kWhL^{-1}order^{-1}$). Above results show that $BaFe_2O_4$/rGO is more energy efficient than GO, reason could be more reactive site and generation of radical for photodegradation of such low concentration organic pollutant. For solar driven system, energy efficiency was quantified during UV treatment. Evidently, EEO of GO and $BaFe_2O_4$/rGO was ranging from 0.59 to 1.71 kW h L^{-1} $order^{-1}$ and 0.76 to 1.1 4 kW h L^{-1} $order^{-1}$, respectively. This higher EEO values of visible treatment could enhance the efficiency of solar treatment (45% visible and 4% UV) (Santiago-Morales et al., 2013). Additionally, reusability of GO and $BaFe_2O_4$/rGO was also investigated, and results were showed good stability even after 3 cycle of $BaFe_2O_4$/rGO (Fig.5d).

4. Conclusion

In this study, synthesized $BaFe_2O_4$/rGO showed enhanced catalytic activity for degradation of CHD in comparison to GO. The structural properties were affected by doping of Ba^{2+} showed decreased band energy of catalyst, which enhanced the photocatalytic degradation of CHD. Characterization results (EDS, XPS and XRD) confirm the crystallinity of the structure and doping on the surface of sample that may favour the photocatalytic degradation of CHD by separation of charge carrier. The result of kinetic studies showed that pseudo first order kinetic model was well fitted, based on the rate constant and R^2 values. The trapping experiment tests demonstrated that the major reactive oxygen species are $^{\bullet}OH$ radicals and photogenerated electrons for CHD degradation. Based on intermediate analysis as well as reduction in TOC and UV_{254}, it was observed that GO and $BaFe_2O_4$/rGO decompose complex long chain into shorter chain species, thus their bacterial toxicity was also reduced during photocatalysis process. The efficiency of as prepared catalyst was examined in the use of energy and the results are higher than previous studies due to the removal of refractory pollutant in the lower

concentration. But comparative studies demonstrated that $BaFe_2O_4$/rGO would be the potential catalyst for solar-driven photocatalysis and maintain the sustainability. Overall results suggested that application of modified $BaFe_2O_4$/rGO photocatalyst for removal and efficient degradation of antibiotic pollutants could be achieved through adsorption and photocatalysis approach. Thus, the practical applicability of this catalyst could be exploited for significant removal of hydrophobic organic pollutant form others industrial wastewater.

Acknowledgement:

The authors are very thankful for the financial support from Indian Institute of Technology (Indian School of Mines), Dhanbad under a Junior Research Fellowship scheme funded by Ministry of Human Resource Development (MHRD), Government of India, New Delhi to carry out this research work. We would also like to acknowledge Aneek Kulia and Soni Kumari for their valuable time in data interpretation and formatting of the manuscript and Nanotechnology Research Centre (NRC), SRMIST for providing the instrumentation facilities.

Ethics approval and consent to participate.

Not applicable

Consent for publication

Not applicable

CRediT authorship contribution statement

Ms. Astha Singh: All experiment, analysis and interpretation of results, Conceptualization, Methodology, Investigation, Formal analysis & Writing-Original Draft. (First Author)

Prof. Brijesh Kumar Mishra: Supervision, Conceptualization, Review &Editing. (Corresponding Author)

Funding

Funding information is not applicable.

Competing interests

The authors declare that they have no competing interests.

Availability of data and materials

All data generated or analysed during this study are included in this published article [and its supplementary information files].

Declaration of competing interest

The authors declare that they have no known competing financial interests or personal relationships that could have appeared to influence the work reported in this paper.

5. References

Aboubaraka, A.E., Aboelfetoh, E.F., Ebeid, E.Z.M., 2017. Coagulation effectiveness of graphene oxide for the removal of turbidity from raw surface water. Chemosphere 181, 738–746. https://doi.org/10.1016/j.chemosphere.2017.04.137

Azarpira, H., Sadani, M., Abtahi, M., Vaezi, N., Rezaei, S., Atafar, Z., Mohseni, S.M., Sarkhosh, M., Ghaderpoori, M., Keramati, H., Hosseini Pouya, R., Akbari, A., fanai, V., 2019. Photo-catalytic degradation of triclosan with UV/iodide/ZnO process: Performance, kinetic, degradation pathway, energy consumption and toxicology. J. Photochem. Photobiol. A Chem. 371, 423–432. https://doi.org/10.1016/j.jphotochem.2018.10.041

Bai, X., Du, Y., Hu, X., He, Y., He, C., Liu, E., Fan, J., 2018. Synergy removal of Cr (VI) and organic pollutants over RP-MoS2/rGO photocatalyst. Appl. Catal. B Environ. 239, 204–213. https://doi.org/10.1016/j.apcatb.2018.08.016

Casbeer, E., Sharma, V.K., Li, X.Z., 2012. Synthesis and photocatalytic activity of ferrites under visible light: A review. Sep. Purif. Technol. 87, 1–14. https://doi.org/10.1016/j.seppur.2011.11.034

Chen, Y., Zhang, X., Wang, L., Cheng, X., Shang, Q., 2020. Rapid removal of phenol/antibiotics in water by Fe-(8-hydroxyquinoline-7-carboxylic)/TiO2 flower composite: Adsorption combined with photocatalysis. Chem. Eng. J. 402. https://doi.org/10.1016/j.cej.2020.126260

Das, R., Sarkar, S., Bhattacharjee, C., 2014. Photocatalytic degradation of chlorhexidine-A chemical assessment and prediction of optimal condition by response surface methodology. J. Water Process Eng. 2, 79–86. https://doi.org/10.1016/j.jwpe.2014.05.005

El-Sheikh, S.M., Khedr, T.M., Hakki, A., Ismail, A.A., Badawy, W.A., Bahnemann, D.W., 2017. Visible light activated carbon and nitrogen co-doped mesoporous TiO2as efficient photocatalyst for degradation of ibuprofen. Sep. Purif. Technol. 173, 258–268. https://doi.org/10.1016/j.seppur.2016.09.034

Fidelis, M.Z., Abreu, E., Dos Santos, O.A.A., Chaves, E.S., Brackmann, R., Dias, D.T., Lenzi, G.G.,

2019. Experimental design and optimization of triclosan and 2.8-diclorodibenzeno-p-dioxina degradation by the Fe/Nb 2 O 5 /UV system. Catalysts 9, 1–18. https://doi.org/10.3390/catal9040343

Han, J.K., Song, D.S., Lim, Y.R., Song, W., Myung, S., Lee, S.S., An, K.S., Jung, H.K., Santucci, S., Esposito, V., Lim, J., 2021. In-depth exploration of the synergistic interplay between perovskite barium titanate nanoparticles and two-dimensional graphene oxide for flexible piezoelectric nanogenerators. Appl. Surf. Sci. 538, 147962. https://doi.org/10.1016/j.apsusc.2020.147962

Hu, Z., Ge, M., Guo, C., 2020. Efficient removal of levofloxacin from different water matrices via simultaneous adsorption and photocatalysis using a magnetic Ag3PO4/rGO/CoFe2O4 catalyst. Chemosphere 128834. https://doi.org/10.1016/j.chemosphere.2020.128834

Li, M. fang, Liu, Y. guo, Zeng, G. ming, Liu, N., Liu, S. bo, 2019. Graphene and graphene-based nanocomposites used for antibiotics removal in water treatment: A review. Chemosphere 226, 360–380. https://doi.org/10.1016/j.chemosphere.2019.03.117

Nasseh, N., Taghavi, L., Barikbin, B., Nasseri, M.A., 2018. Synthesis and characterizations of a novel FeNi3/SiO2/CuS magnetic nanocomposite for photocatalytic degradation of tetracycline in simulated wastewater. J. Clean. Prod. 179, 42–54. https://doi.org/10.1016/j.jclepro.2018.01.052

Nidhi, K., Indrajeet, S., Khushboo, M., Gauri, K., Sen, D.J., 2011. Hydrotropy: A promising tool for solubility enhancement: A review. Int. J. Drug Dev. Res. 3, 26–33. https://doi.org/10.1002/jps

Priya, T., Prakash, P., Mishra, B.K., 2018. Understanding the coagulant activity of zirconium oxychloride to control THMs formation using response surface methodology. Ecotoxicol. Environ. Saf. 159, 28–37. https://doi.org/10.1016/j.ecoenv.2018.04.036

Roonasi, P., Mazinani, M., 2017a. Synthesis and application of barium ferrite/activated carbon composite as an effective solar photocatalyst for discoloration of organic dye contaminants in wastewater. J. Environ. Chem. Eng. 5, 3822–3827. https://doi.org/10.1016/j.jece.2017.07.035

Roonasi, P., Mazinani, M., 2017b. Synthesis and application of barium ferrite/activated carbon composite as an effective solar photocatalyst for discoloration of organic dye contaminants in wastewater. J. Environ. Chem. Eng. 5, 3822–3827. https://doi.org/10.1016/j.jece.2017.07.035

Santiago-Morales, J., Gómez, M.J., Herrera-López, S., Fernández-Alba, A.R., García-Calvo, E., Rosal, R., 2013. Energy efficiency for the removal of non-polar pollutants during ultraviolet irradiation, visible light photocatalysis and ozonation of a wastewater effluent. Water Res. 47, 5546–5556. https://doi.org/10.1016/j.watres.2013.06.030

Schneider, J., Matsuoka, M., Takeuchi, M., Zhang, J., Horiuchi, Y., Anpo, M., Bahnemann, D.W., 2014. Understanding TiO $_2$ Photocatalysis: Mechanisms and Materials. Chem. Rev. 114, 9919–9986. https://doi.org/10.1021/cr5001892

Singh, M., Kaushal, S., Singh, P., Sharma, J., 2018. Boron doped graphene oxide with enhanced photocatalytic activity for organic pollutants. J. Photochem. Photobiol. A Chem. 364, 130–139.

https://doi.org/10.1016/j.jphotochem.2018.06.002
Sonal, S., Prakash, P., Mishra, B.K., Nayak, G.C., 2020. Synthesis, characterization and sorption studies of a zirconium(IV) impregnated highly functionalized mesoporous actIVated carbonsb. RSC Adv. 10, 13783–13798. https://doi.org/10.1039/c9ra10103a
Sonal, S., Singh, A., Mishra, B.K., 2018. Decolorization of reactive dye Remazol Brilliant Blue R by zirconium oxychloride as a novel coagulant: Optimization through response surface methodology. Water Sci. Technol. 78, 379–389. https://doi.org/10.2166/wst.2018.307
Sousa, C.P., de Oliveira, R.C., Freire, T.M., Fechine, P.B.A., Salvador, M.A., Homem-de-Mello, P., Morais, S., de Lima-Neto, P., Correia, A.N., 2017. Chlorhexidine digluconate on chitosan-magnetic iron oxide nanoparticles modified electrode: Electroanalysis and mechanistic insights by computational simulations. Sensors Actuators, B Chem. 240, 417–425. https://doi.org/10.1016/j.snb.2016.08.181
Thakur, K., Kandasubramanian, B., 2019. Graphene and Graphene Oxide-Based Composites for Removal of Organic Pollutants: A Review. J. Chem. Eng. Data 64, 833–867. https://doi.org/10.1021/acs.jced.8b01057
Wang, H., Zhang, M., He, X., Du, T., Wang, Y., Li, Y., Hao, T., 2019. Facile prepared ball-like TiO2 at GO composites for oxytetracycline removal under solar and visible lights. Water Res. 160, 197–205. https://doi.org/10.1016/j.watres.2019.05.073
Wang, X., Xu, G., Tu, Y., Wu, D., Li, A., Xie, X., 2021. BiOBr/PBCD-B-D dual-function catalyst with oxygen vacancies for Acid Orange 7 removal: Evaluation of adsorption-photocatalysis performance and synergy mechanism. Chem. Eng. J. 411, 128456. https://doi.org/10.1016/j.cej.2021.128456
Wang, Z.L., Xu, D., Huang, Y., Wu, Z., Wang, L.M., Zhang, X.B., 2012. Facile, mild and fast thermal-decomposition reduction of graphene oxide in air and its application in high-performance lithium batteries. Chem. Commun. 48, 976–978. https://doi.org/10.1039/c2cc16239c
Yuan, Q., Zhang, D., Yu, P., Sun, R., Javed, H., Wu, G., Alvarez, P.J.J., 2020. Selective Adsorption and Photocatalytic Degradation of Extracellular Antibiotic Resistance Genes by Molecularly-Imprinted Graphitic Carbon Nitride. Environ. Sci. Technol. 54, 4621–4630. https://doi.org/10.1021/acs.est.9b06926
Zhang, X., Shen, J., Zhuo, N., Tian, Z., Xu, P., Yang, Z., Yang, W., 2016. Interactions between Antibiotics and Graphene-Based Materials in Water: A Comparative Experimental and Theoretical Investigation. ACS Appl. Mater. Interfaces 8, 24273–24280. https://doi.org/10.1021/acsami.6b09377
Zhu, C., Chen, X., Ma, J., Gu, C., Xian, Q., Gong, T., Sun, C., 2018. Carbon Nitride-Modified Defective TiO2- x@Carbon Spheres for Photocatalytic H2 Evolution and Pollutants Removal:

643 Synergistic Effect and Mechanism Insight. J. Phys. Chem. C 122, 20444–20458.
644 https://doi.org/10.1021/acs.jpcc.8b06624
645 Zwiener, C., Frimmel, F.H., 2000. Oxidative treatment of pharmaceuticals in water. Water Res. 34,
646 1881–1885. https://doi.org/10.1016/S0043-1354(99)00338-3
647

Figures

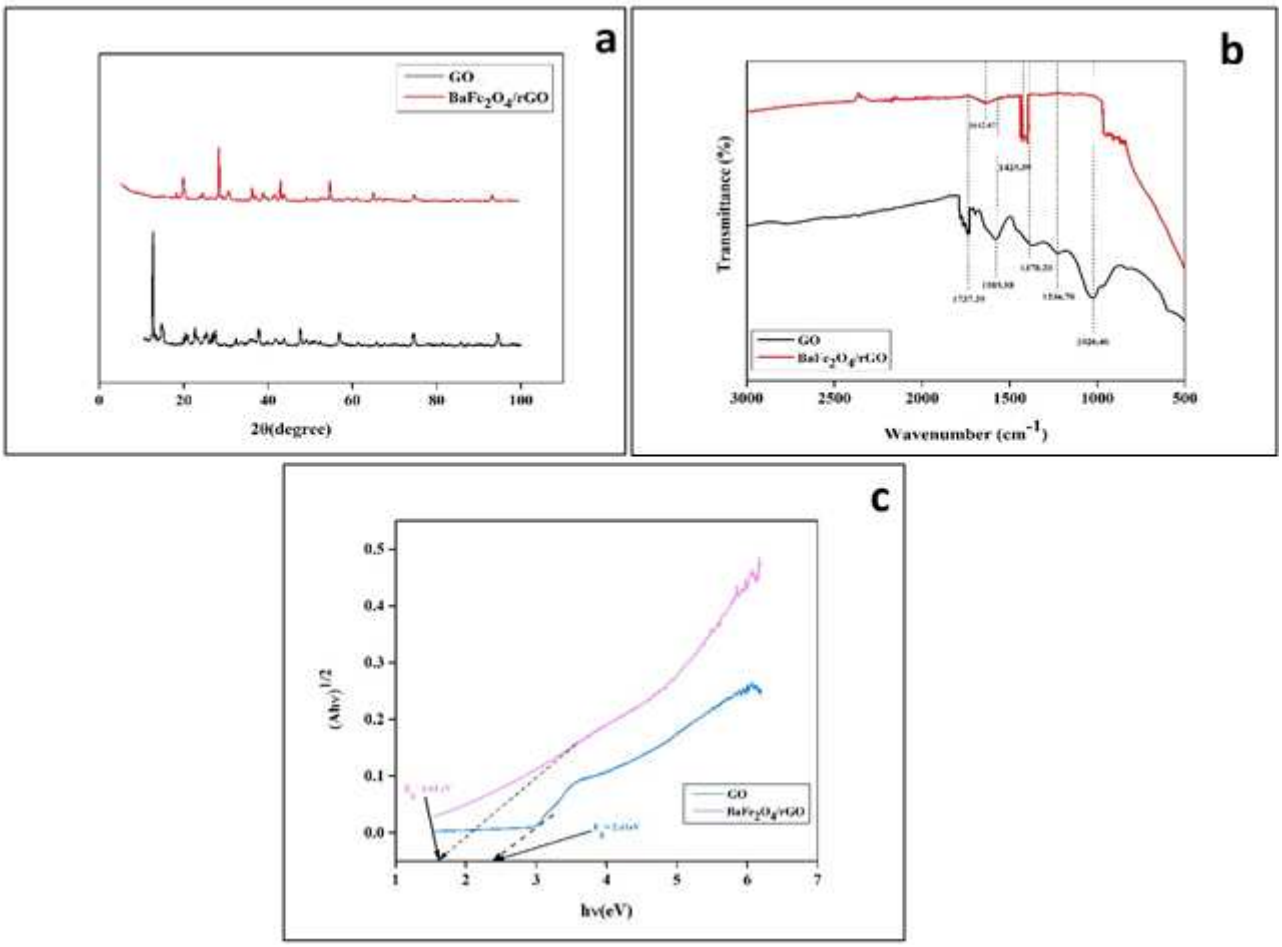

Figure 1

a) XRD patterns; b) FTIR spectra and c) UV-vis diffuse reflectance spectra of GO and BaFe2O4/rGO.

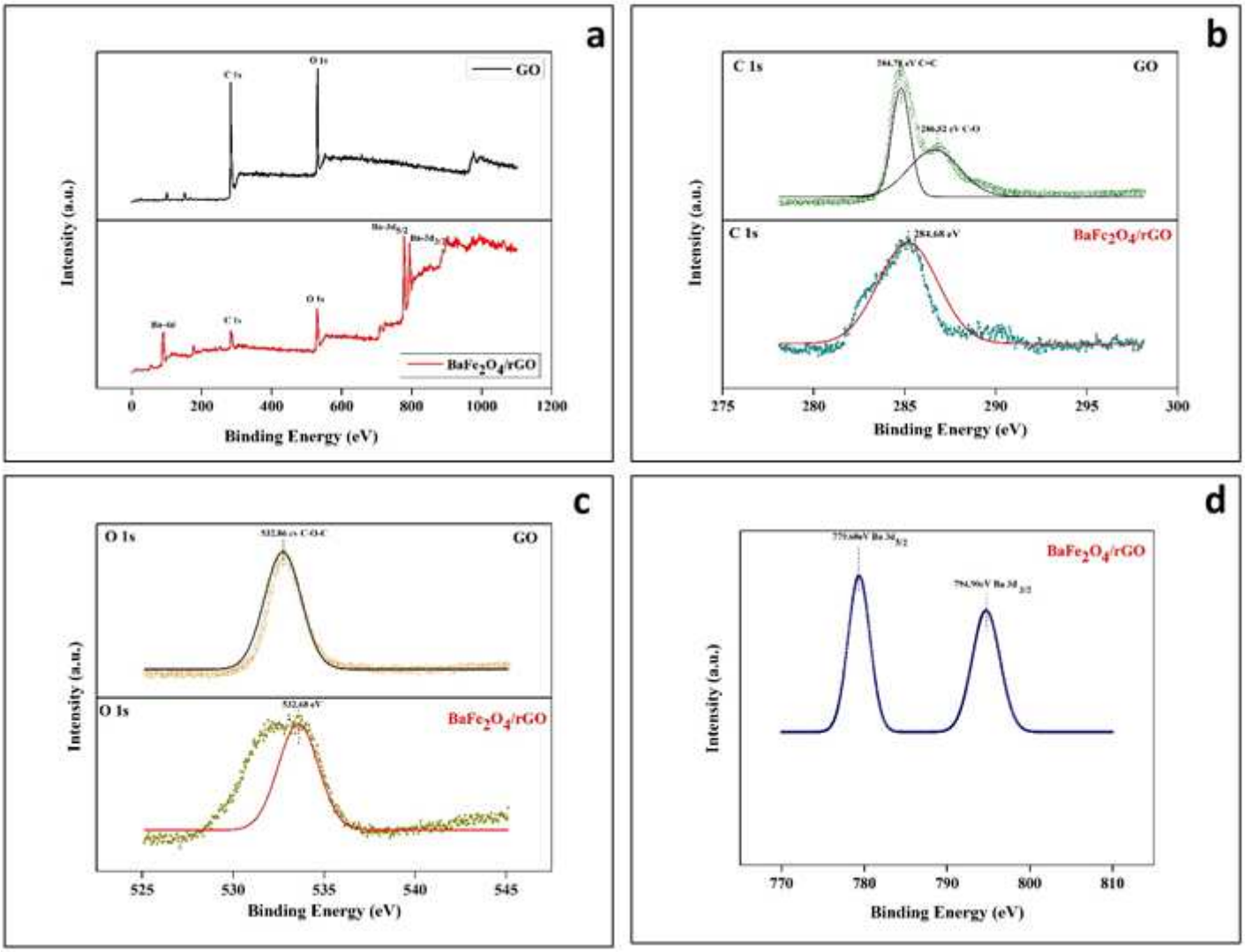

Figure 2

a) Full scan spectra and extended high-resolution b) C 1s; c) O 1s and d) Ba 3d spectra of GO and BaFe2O4/rGO.

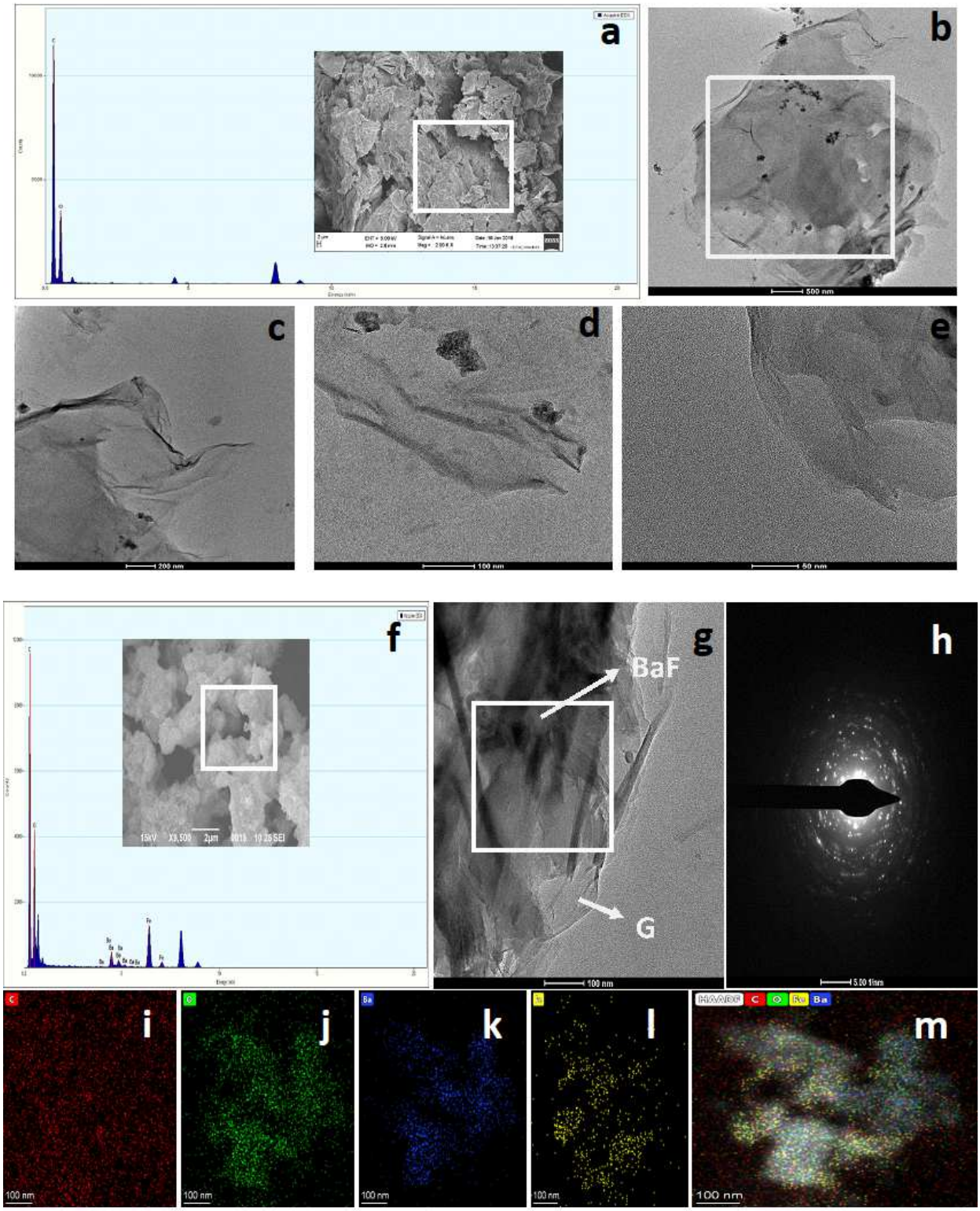

Figure 3

SEM, TEM and EDS images of photocatalysts (a-e) GO; and (f-m) BaFe2O4/rGO.

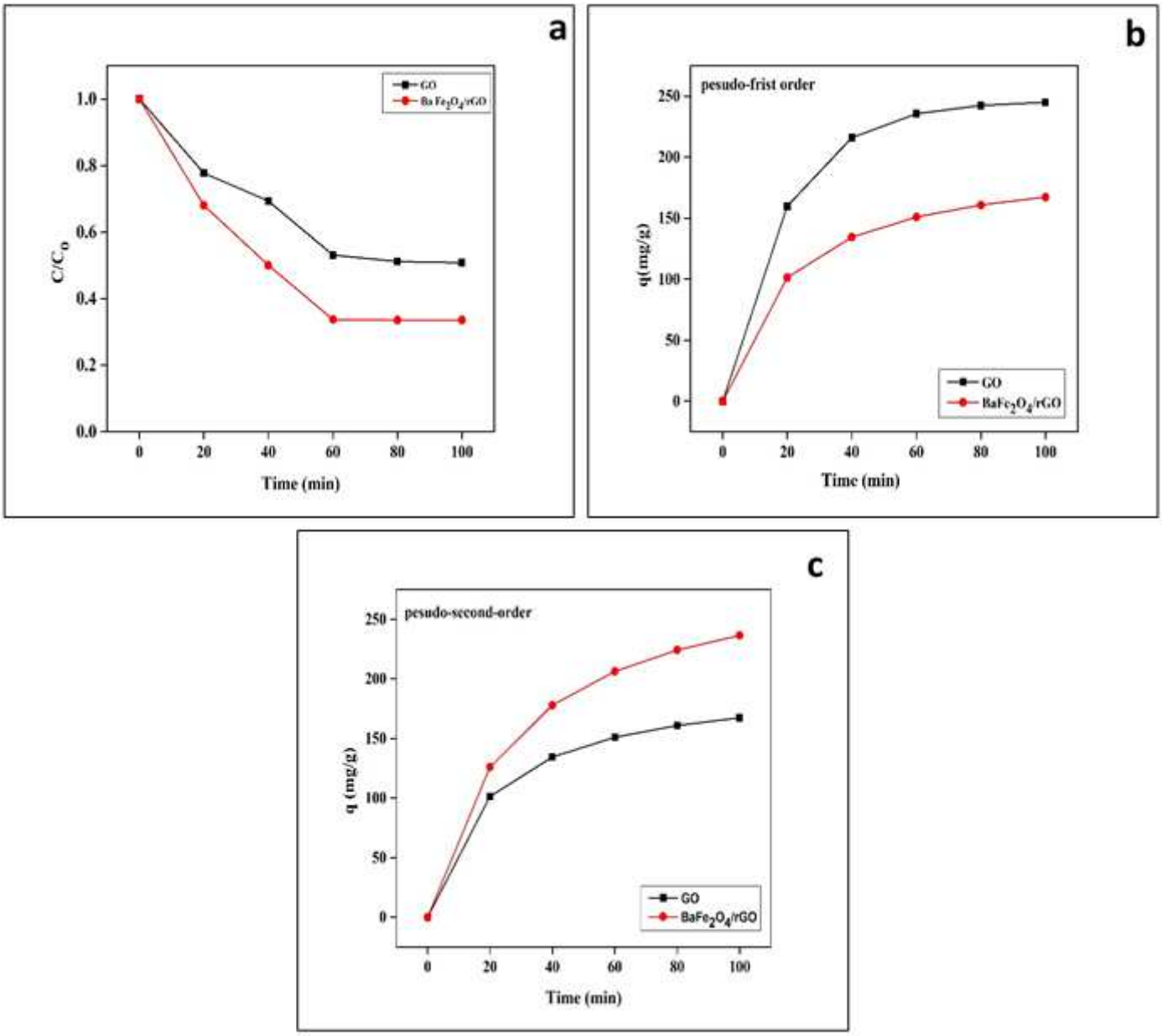

Figure 4

a) Adsorption of CHD at optimized condition; b) pseudo-first order model; and c) pseudo-second order model for GO and BaFe2O4/rGO.

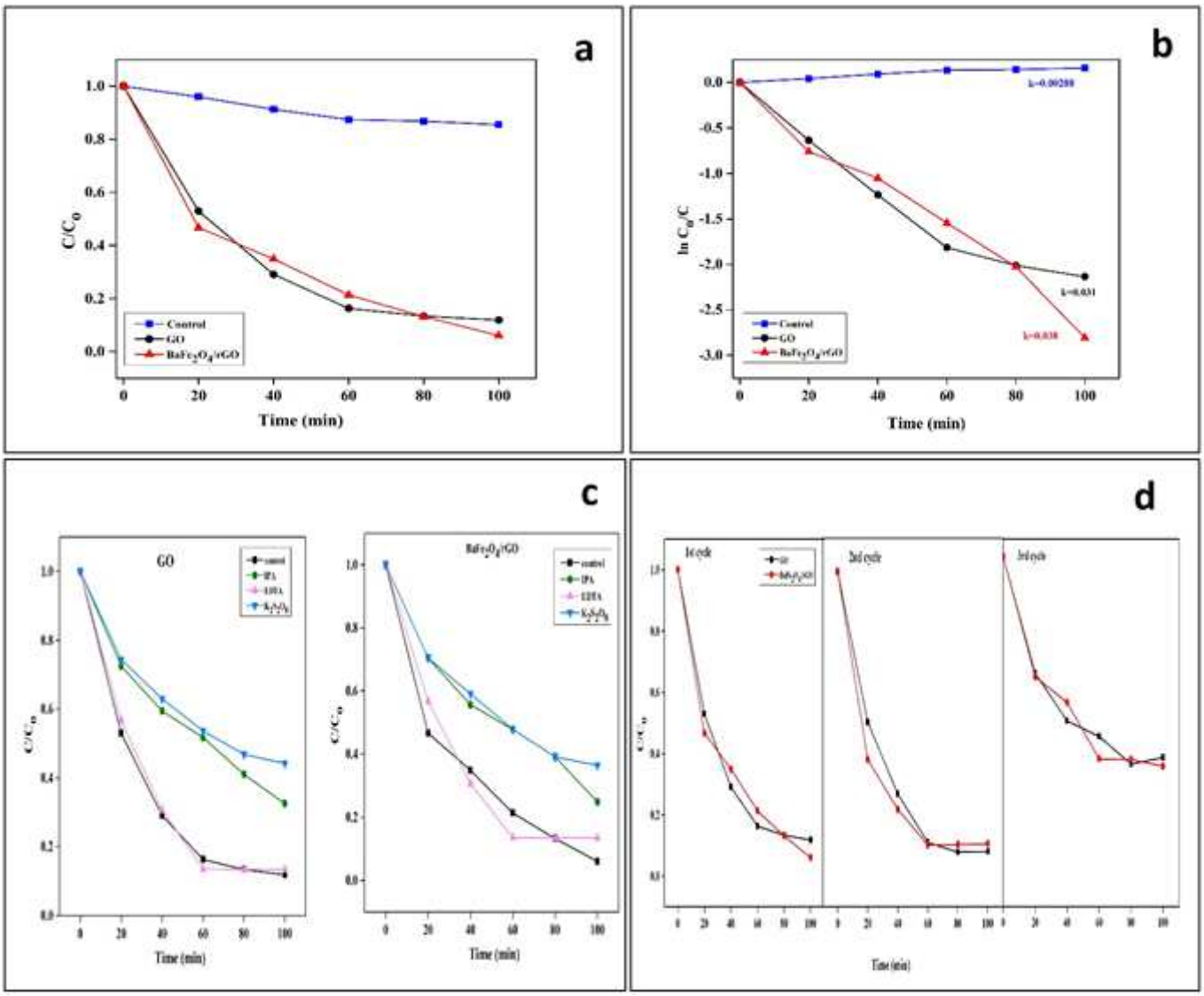

Figure 5

a) Photocatalytic degradation of CHD at optimized condition; b) pseudo-first order kinetics; c) trapping experiment of active species; and d) reusability experiment of GO and BaFe2O4/rGO mediated photocatalytic degradation of CHD.

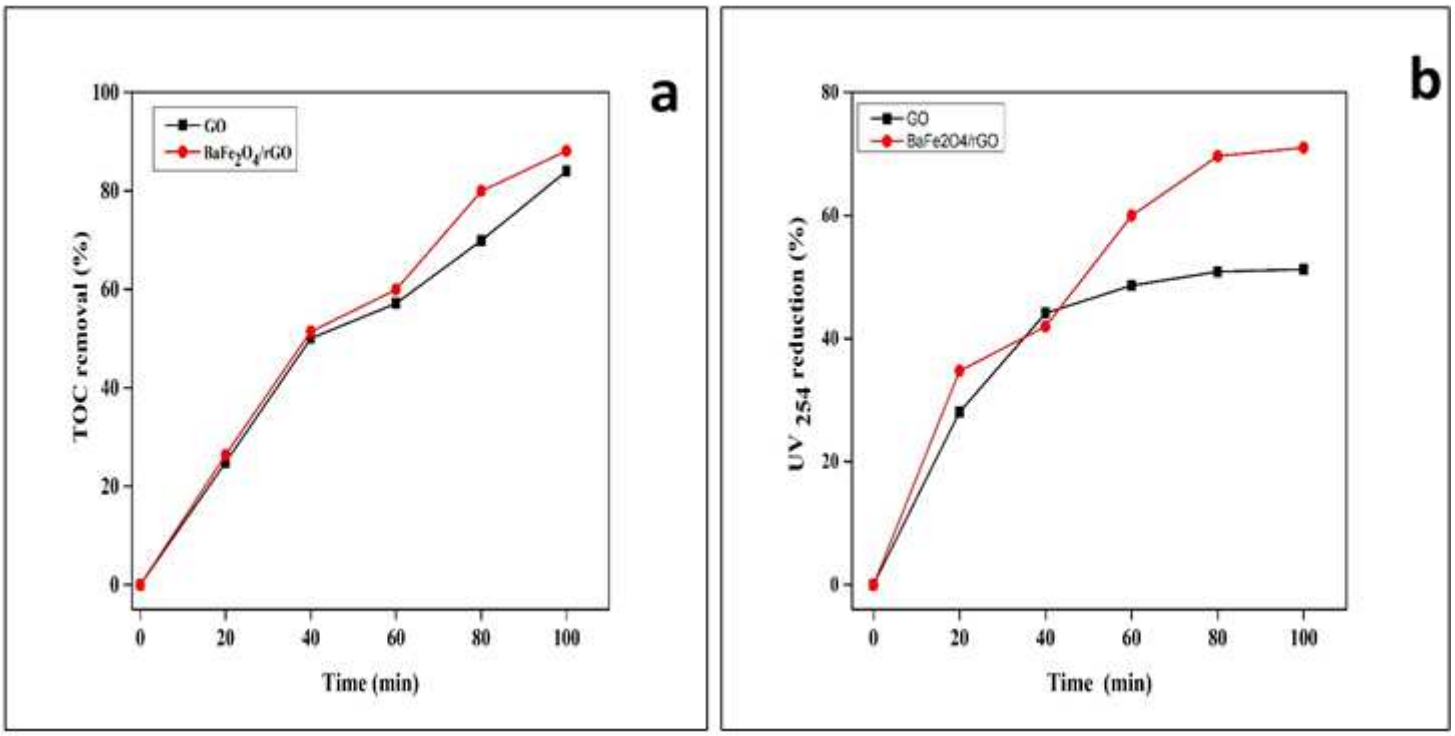

Figure 6

a) TOC removal and; b) UV absorbance reduction in GO and BaFe2O4/rGO mediated photocatalytic degradation of CHD at optimized condition.

Supplementary Files

This is a list of supplementary files associated with this preprint. Click to download.

- GA.png
- Supplementary.docx